A New Hybrid Particle-Puff Approach to Atmospheric Dispersion Modelling, Implemented in the Danish Emergency Response Model of the Atmosphere (DERMA)

Kasper Skjold Tølløse[1,2] and Jens Havskov Sørensen[1]

[1]Danish Meteorological Institute
[2]Niels Bohr Institute, University of Copenhagen

Correspondence: Kasper Skjold Tølløse (ktoe@dmi.dk)

Abstract. The Danish Emergency Response Model of the Atmosphere (DERMA) is a Lagrangian puff model originally developed for long-range dispersion modelling, on distances longer than roughly 50 km from the source. The model is used operationally as part of Danish emergency preparedness for the prediction of atmospheric dispersion in case of nuclear accidents, airborne spread of animal diseases, and ash from volcanic eruptions. To be able to simulate dispersion on shorter spatial scales, a new description of turbulent diffusion has been developed and implemented in DERMA, combining a stochastic particle approach with a classic puff model. Further, updates have been made to the parameterizations of the turbulent wind fluctuations and Lagrangian time scales, the boundary layer height, and the initial plume rise due to heat release. These improvements allow for a more realistic description of turbulent diffusion near the release location, while an updated version of the existing turbulence description is used at longer distances. The new version of DERMA is evaluated against three different tracer gas experiments: the European Tracer Experiment (ETEX), the Øresund experiment, and the Kincaid experiment. The results indicate that the new particle-puff hybrid approach gives more accurate predictions, especially on shorter spatial scales while a small improvement is also observed for long-range dispersion.

1 Introduction

Lagrangian atmospheric dispersion models can be divided into two categories, stochastic particle models and puff models. Both rely on modelling the positions of particles following Lagrangian trajectories. In stochastic particle models, each particle follows a turbulent trajectory estimated using stochastic differential equations, and the resulting concentration field is then determined by the spread of particles. These models typically make as few assumptions as possible and, therefore, they are capable of making physically accurate simulations. However, a large number of particles is needed to accurately resolve the fine structures of the three-dimensional plume, which makes this type of model computationally expensive. Further, as discussed by Stohl et al. (2005), short advection time steps, on the order of a few seconds, may be necessary in order to resolve the turbulent trajectories in all conditions. Some examples of stochastic particle models are the models FLEXPART (Stohl et al., 2005; Pisso et al., 2019), HYSPLIT (Draxler and Hess, 1997), and NAME (Jones et al., 2004). The latter uses a hybrid particle-

puff description for short-range modelling, while only on longer distances the particles are assumed to be point concentrations (Jones et al., 2004).

The Lagrangian puff approach is a computationally cheaper alternative, where each puff instead follows the average wind field, and turbulent diffusion is assumed to follow a Gaussian distribution locally around each puff's centroid. Some examples are the models CALPUFF (Scire et al., 2000), DIPCOT (Andronopoulos et al., 2009), RIMPUFF (Thykier-Nielsen et al., 1999), and DERMA (Sørensen et al., 2007). In this type of model, much fewer particles are used compared to the stochastic particle models, and the Gaussian concentration distributions then "fill the gaps" between particle locations. For relatively young puffs, this assumption works quite well, but when the puffs grow beyond a certain size, the vertical wind shear may cause puffs to stretch over different flow regimes, which would in reality distort the Gaussian shape (Jones et al., 2004). A typical solution for this problem, used in e.g. NAME, CALPUFF, and RIMPUFF, is the use of puff splitting, i.e. a puff that grows too large is split into several smaller puffs at different heights (Jones et al., 2004; Scire et al., 2000; Thykier-Nielsen et al., 1999). This ensures a more physical behavior, but it introduces new challenges due to the continuously increasing number of puffs (Draxler and Hess, 1997). An alternative approach, described further below, is to introduce stochastic movement, which exposes each puff to the wind at different heights and, thereby, leads to a more realistic dispersion pattern.

In addition to these two model types, different hybrid formulations have been proposed combining elements from both stochastic particle models and puff models. As already mentioned, the NAME model employs such an approach on shorter scales, but also the models DIPCOT and DERMA combine the puff approach with a stochastic displacement of puffs (Andronopoulos et al., 2009; Sørensen et al., 2007). Another example of a hybrid formulation is the Puff-Particle-Model (PPM) suggested by De Haan and Rotach (1998). In the PPM, the turbulent effects are separated into two distinct physical processes, a meandering part (larger scale than the puff) and a relative dispersion around each puff centroid, represented by the puff growth. However, in order to keep puffs smaller than the meandering scales, PPM uses more puffs and more frequent puff splitting than in regular puff models and should be considered a compromise between the two model types, with respect to both accuracy and efficiency (De Haan and Rotach, 1998).

In the currently operational version of the DERMA model, v1.0.0, complete mixing throughout the boundary layer is assumed, which means that the concentration field of a puff is only assumed Gaussian horizontally, while it is described by a uniform distribution vertically for puffs inside the planetary boundary layer (PBL). Thus, as discussed above, the puffs in DERMA are likely to stretch over different flow regimes. However, a vertical stochastic transport scheme inside the PBL is used as an alternative to puff splitting; by randomly moving puff centroids inside the PBL to new vertical positions, each puff is exposed to the vertical wind shear over time (Sørensen, 1998; Sørensen et al., 2007). Despite this relatively simple formulation, DERMA was ranked as one of the best performing models in the ETEX model evaluation (Graziani et al., 1998).

DERMA is currently used operationally for a number of purposes for Danish emergency preparedness including nuclear accidents, volcanic eruptions, and airborne animal diseases (Sørensen et al., 2000, 2001; Mikkelsen et al., 2003; Gloster et al., 2010; Hoe et al., 2002). In recent years, the model has further been used in different research projects about inverse modelling for source localization and source term reconstruction for a nuclear accident (Sørensen, 2018; Tølløse et al., 2021; Tølløse and Sørensen, 2022). The DERMA model was specifically designed for long-range dispersion modelling, and some assumptions

are not applicable on shorter scales. The aim of this study is to develop a new description of turbulent diffusion, which enables the new version of the model, DERMA v2.0.0, to accurately predict dispersion closer to the release location.

In this study, we develop a new hybrid particle-puff approach, which separates the turbulent diffusion in a stochastic part and a puff part. On shorter scales, the separation is based on the size of the puff compared to the length scale associated with the largest turbulent eddies. This is conceptually similar to the approach by De Haan and Rotach (1998) used in the PPM. However, on longer scales, the stochastic part works as compensation for the fact that the puff assumption fails for physically large puffs, similar to the formulation in DERMA v1.0.0. In addition to the new description of turbulent diffusion, several updates have been made to DERMA, which are described in detail in Section 2. Further, the new particle-puff approach has been evaluated against three tracer gas experiments; the European Tracer Experiment (ETEX), the Øresund experiment, and the Kincaid experiment. Details on the evaluation process and the results are presented in Section 3. Finally, a summary and the conclusions are presented in Section 4.

2 Model description

In this section, a detailed description of all the new elements in DERMA is given. For a more general description of the DERMA model, see Sørensen (1998); Baklanov and Sørensen (2001); Sørensen et al. (2007). In Section 2.1, the new hybrid particle-puff formulation is described. Next, Section 2.2 describes the updates made to the PBL parameterization including a new parameterization of turbulent wind fluctuations, Lagrangian time scales, and PBL height. Finally, Section 2.3 describes the Concawe and Briggs plume rise algorithms, which have also been implemented.

2.1 Hybrid particle-puff description

As discussed previously, one of the shortcomings of the puff model approach is that puffs will eventually grow larger than the characteristic length scale of the vertical wind shear, causing the puff assumption to fail. Further, the smallest puffs may be smaller than the largest turbulent eddies in some conditions. Therefore, at the early stages, the puffs should be displaced by these, until they grow larger than the eddies themselves. In this study, we develop a simple hybrid approach, which attempts to target both of these issues. For small puffs, the hybrid approach is designed such that puffs are displaced by the largest eddies, while smaller eddies cause the puffs to grow, and for large puffs, a stochastic displacement will expose puffs to the wind shear hence avoiding the need for puff splitting.

As in DERMA v1.0.0, the puffs grow according to the formulation by Gifford (1984)

$$\sigma_i^2 = 2K_i t_{L_{u_i}} \left\{ \tau_i - \left(1 - e^{-\tau_i}\right) - \frac{1}{2}\left(1 - e^{-\tau_i}\right)^2 \right\}, \tag{1}$$

where σ_i is the puff's standard deviation along the x_i-axis, K_i is the turbulent diffusivity, $t_{L_{u_i}}$ is the Lagrangian time scale, i.e. the auto-correlation time for the velocity fluctuations, t is the age of the puff, and $\tau_i = t/t_{L_{u_i}}$. In DERMA v2.0.0, we instead consider the time derivative of Equation 1

$$\frac{\partial}{\partial t}\sigma_i^2 = 2\sigma_{u_i}^2 t_{L_{u_i}} \left(1 - e^{-\tau_i}\right)^2,$$

where we have used the relation between the diffusivity and the turbulent velocity scale $K_i = \sigma_{u_i}^2 t_{L_{u_i}}$. This can be written in the numerical form

$$\Delta\sigma_i^2(t+\Delta t/2) = 2\sigma_{u_i}^2(t) t_{L_{u_i}}(t)\Delta t \left(1 - \exp\left(-\frac{t+\Delta t/2}{t_{L_{u_i}}(t)}\right)\right)^2, \quad (2)$$

which is evaluated at the time $t+\Delta t/2$, i.e. halfway between the two neighboring discrete time steps. To avoid double-counting the effects of turbulence, Eq. (2) must describe the combined effects of the puff growth and stochastic parts of the turbulent diffusion.

We consider the case where puffs have been dispersed around a point following mean wind trajectories $\mathbf{x}_t$ and assume that the puff centroids, $\mathbf{x}_p$, are distributed according to Gaussian particle distributions in all three spatial dimensions. Thus, along the x_i-axis puff centroids are distributed as $f(x_i) = \mathcal{N}(x_{i,t}, \sigma_{i,part})$. Further, the concentration field from each puff around its centroid is assumed to follow the Gaussian distribution $g(x_i) = \mathcal{N}(0, \sigma_{i,puff})$.

The resulting concentration distribution can be obtained by calculating the convolution of the two distributions (Bromiley, 2003)

$$f(x_i) \circledast g(x_i) = \int_{-\infty}^{\infty} f(x_i')g(x_i - x_i')\mathrm{d}x_i' = \mathcal{N}\left(x_{i,t}, \sqrt{\sigma_{i,part}^2 + \sigma_{i,puff}^2}\right).$$

Next, we impose the requirement that the resulting concentration distribution should be identical to the Gaussian distribution $\mathcal{N}(x_{i,t}, \sigma_i)$, with σ_i from Eq. (1), in accordance with the formulation by Gifford (1984). To ensure this, the increment of the variances for the distributions $f(x_i)$ and $g(x_i)$ must fulfill the following requirements at every numerical time step

$$\begin{aligned} \Delta\sigma_{i,puff}^2 &= \beta_i^2 \Delta\sigma_i^2, \\ \Delta\sigma_{i,part}^2 &= (1-\beta_i^2)\Delta\sigma_i^2, \end{aligned} \quad (3)$$

where $\Delta\sigma_i^2$ is given by Eq. (2), and $\beta_i \in [0,1]$ is a parameter determining how much stochastic movement is used. If $\beta_i = 1$, the model is a classical puff model, while in the case $\beta_i = 0$, the turbulent diffusion is described purely by the stochastic transport and the puffs keep their initial sizes.

The indices $_{i,part}$ and $_{i,puff}$ indicate the parts of the turbulence accounted for by stochastic displacement and puff growth along the x_i-axis, respectively. Hence, during each numerical time step, a puff's variance grows with $\Delta\sigma_{i,puff}^2$, Eq. (3), while its centroid is moved by a random walk with step size $\Delta\sigma_{i,part}$, Eq. (3). If the turbulence is Gaussian and if there is no vertical wind shear, any value of β_i should be valid, provided there is a sufficient number of particles. However, since vertical wind shear is a fundamental feature of the atmosphere, especially in the PBL, the addition of a stochastic element to the turbulence description should improve the performance by exposing puffs to the winds at different heights.

2.1.1 Determining β_i

Early in the life of a puff, the puff might be smaller than the largest turbulent eddies and, therefore, we can make a physical distinction between the particle part and the puff part. Although our approach is different, this distinction is conceptually

similar to the approach by De Haan and Rotach (1998). Here, we use the fraction of the turbulent kinetic energy (TKE) on larger scales than the puff itself. Thus, we first consider the TKE spectrum (Kolmogorov, 1941)

$$TKE(k) \propto \varepsilon^{2/3} k^{-5/3}, \tag{4}$$

where ε is the TKE dissipation rate, $k = \frac{2\pi}{\lambda}$ is the wave number, and the wavelength λ corresponds to the length scale associated with the turbulent eddies. In reality, $k = |\mathbf{k}|$, where $\mathbf{k}$ is the three-dimensional wave number, which is of course not necessarily equal in all physical dimensions. However, for this purpose, we assume that the relation, Eq. (4) holds in each spatial dimension individually. Thus, assuming that the puff has the spatial extent σ_i along the x_i-axis, we can estimate the fraction of the TKE accounted for by eddies on smaller spatial scales than the puff itself

$$\frac{TKE_{puff}}{TKE} = \frac{\int_{\frac{2\pi}{\sigma_i}}^{\infty} TKE(k_i)\mathrm{d}k_i}{\int_{\frac{2\pi}{l_i}}^{\infty} TKE(k_i)\mathrm{d}k_i} = \left(\frac{\sigma_i}{l_i}\right)^{2/3}, \tag{5}$$

where l_i is the length scale associated with the largest eddies along the i'th physical dimension, which is estimated as $l_i = \sigma_{u_i} t_{L_{u_i}}$.

The fraction in Eq. (5) seems like a natural choice for the value of β_i^2, except that when the puff grows larger than the largest eddies, the particle part will then naturally die out. Thus, to ensure that the stochastic part does not vanish, we define

$$\beta_i = \max\left(\beta_{\min}, \left(\frac{\sigma_i}{l_i}\right)^{1/3}\right), \tag{6}$$

where $\beta_{\min} \in [0,1]$ is a hyperparameter that needs to be determined to find the ideal balance between the particle and puff parts. We use $\beta_{\min} = \sqrt{1/2}$, which divides the turbulence evenly between the particle part and the puff part.

It is assumed that puffs inside the boundary layer are reflected both at the surface and at the PBL top. Further, for puffs above the boundary layer, the stochastic part will automatically be turned off by setting $\beta_i = 1$.

2.1.2 Short-range and long-range formulations

The concentration field from a puff in a point (x_p, y_p, z_p) can be written as

$$C_p = \frac{Q_p}{2\pi\sigma_y^2\sigma_z} \exp\left\{-\frac{1}{2}\left(\frac{x-x_p}{\sigma_y}\right)^2 - \frac{1}{2}\left(\frac{y-y_p}{\sigma_y}\right)^2 - \frac{1}{2}\left(\frac{z-z_p}{\sigma_z}\right)^2\right\}, \tag{7}$$

where Q_p is the mass/activity carried by the puff. However, when a puff has grown to a certain size compared to the PBL height, a uniform distribution is assumed vertically, i.e. the formulation from DERMA v1.0.0 is adapted. This happens whenever $\sigma_z \geq h/\alpha$, where h is the PBL height, and α is a hyperparameter determining how fast a puff is assumed to fill out the boundary layer. We use $\alpha = 2$, which means that complete mixing is assumed when $2\sigma_z$ exceeds the PBL height. The reasoning behind this is that, at this stage, the Gaussian distribution is already sufficiently diluted that the surface concentrations are not expected to change dramatically by changing to the uniform distribution. Whenever a puff fulfills this requirement, the concentration

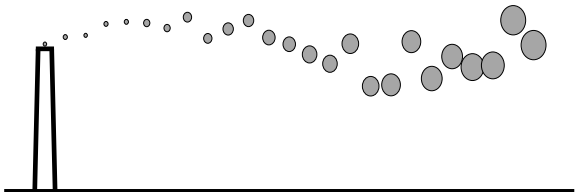

Behavior on short scale

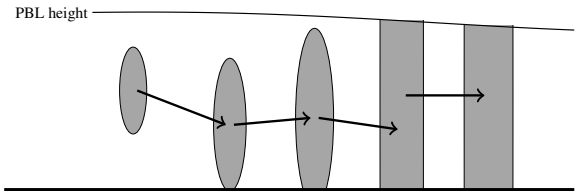

Behavior on transitional scale

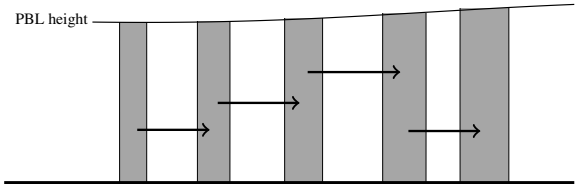

Behavior on long scale

Figure 1. Illustration of the formulation used in DERMA v2.0.0. The upper sketch shows how puffs are released from the top of a stack and are randomly displaced vertically. The middle sketch shows the transition when a puff starts using a uniform concentration distribution in the vertical direction. Finally, the lower sketch shows how the long-range formulation works; puffs assume a uniform vertical distribution inside the PBL, and the height of the puff centroid is displaced vertically with the stochastic transport scheme.

field is instead described by

$$C_p = \frac{Q_p}{2\pi\sigma_y^2 h}\exp\left\{-\frac{1}{2}\left(\frac{x-x_p}{\sigma_y}\right)^2 - \frac{1}{2}\left(\frac{y-y_p}{\sigma_y}\right)^2\right\}\delta(z,h), \tag{8}$$

$$\text{where } \delta(z,h) = \begin{cases} 1 & \text{if } z \le h \\ 0 & \text{if } z > h \end{cases}.$$

This concept is illustrated in Figure 1, where a schematic drawing shows the behavior of the model at short and long scales. This formulation will naturally result in a sharp change in concentration at the top of the boundary layer, which is especially suitable for convective conditions with a capping inversion trapping particles inside the PBL. For stable conditions, the formulation may be less accurate but, as described below, different processes allow puffs to escape the PBL resulting in a smoother transition at the top of the PBL.

When the complete mixing state is reached, the puff is assumed to fill out the boundary layer at all later times, even when the boundary layer grows. Thus, since the puff is no longer growing vertically, all turbulence is assumed to contribute to the stochastic movement, i.e. we set $\beta_z = 0$. Only if the centroid of a completely mixed puff escapes the boundary layer, it will transform back to a Gaussian form in the vertical dimension. The leakage of concentration to the free troposphere can happen in two different ways; (1) if a puff centroid is lifted sufficiently by the mean wind, or (2) if the boundary layer shrinks and, as a result, a puff centroid happens to be above the boundary layer.

This long-range formulation is similar to that of DERMA v1.0.0 but with the improved stochastic transport scheme described above, whereas the old stochastic transport scheme simply assigns a new random height to each puff inside the PBL at every time step (Sørensen et al., 2007).

2.2 Parameterization of boundary layer parameters

The calculation of both the puff part and particle part described above depends on $\sigma_{u_i}^2$ and $t_{L_{u_i}}$, which in turn depend on several boundary layer parameters that are either imported or calculated in DERMA.

From the output of the numerical weather prediction (NWP) model, DERMA imports instantaneous turbulent fluxes of momentum, τ_0, and sensible and latent heat, Q_s and Q_l. From these, the following parameters are calculated (Zannetti, 2013, Ch. 3)

$$L = -\frac{u_*^3 T_v}{\kappa g \left(\overline{w'\theta_v'}\right)_0}, \tag{9}$$

$$u_* = \sqrt{\frac{\tau_0}{\rho}}, \tag{10}$$

$$w_* = \left(\frac{h g \left(\overline{w'\theta_v'}\right)_0}{T_v}\right)^{1/3}, \tag{11}$$

where L is the Obukhov length, which is related to the static stability of the boundary layer, and the friction velocity u_* is assumed the fundamental velocity scale of the non-convective turbulent boundary layer, whereas w_* is the convective velocity scale. Further, ρ is the air density, $g = 9.81\ \mathrm{ms}^{-2}$ is the gravitational acceleration constant, $\kappa = 0.4$ is the von Karman constant, T_v is the surface virtual temperature, and h is the PBL height, which is calculated as described in Section 2.2.1. Finally, $\left(\overline{w'\theta_v'}\right)_0$ is the surface buoyancy flux, i.e. the flux of virtual potential temperature, which can be estimated directly from the imported heat fluxes as $\left(\overline{w'\theta_v'}\right)_0 \approx (Q_s + 0.07Q_l)/(\rho c_p)$, where c_p is the heat capacity at constant pressure (Zannetti, 2013, Ch. 3).

2.2.1 PBL height

The PBL height parameterization is based on the approach by Vogelezang and Holtslag (1996), which relies on a modified form of the Bulk Richardson number

$$Ri(z) = \frac{(g/\Theta_{v,s})(\Theta_v(z) - \Theta_{v,s})z}{U(z)^2 + V(z)^2 + 100u_*^2}, \tag{12}$$

where $\Theta_{v,s}$ is the surface virtual potential temperature, $\Theta_v(z)$ is the virtual potential temperature at height z, and $U(z)$ and $V(z)$ are the horizontal wind components at height z. The PBL height h is set equal to the height z where the requirement $Ri(z) = 0.25$ is obtained for the first time moving upwards from the ground.

2.2.2 Turbulent wind fluctuations

As in DERMA v1.0.0, the constant turbulent diffusivity $K_y = 6 \cdot 10^3 \mathrm{m^2 s^{-1}}$ and corresponding Lagrangian time scale $t_{L_v} = 10^4$ s are assumed for the horizontal diffusion (Sørensen et al., 2007). The vertical component of turbulent velocity fluctuations and the corresponding Lagrangian time scale are parameterized according to the formulations by Hanna (1984). The formulas are given below for the different stability regimes and are valid for puffs within the PBL. For puffs above the boundary layer, we instead use the constant values $\sigma_w = 0.1\ \mathrm{ms^{-1}}$ and $t_{L_w} = 100$ s resulting in a vertical diffusivity of $K_z = 1\ \mathrm{m^2 s^{-1}}$, which was used in the previous version of DERMA and is similar to other models such as NAME, which uses $K_z = 1.5\ \mathrm{m^2 s^{-1}}$ for the free troposphere (Sørensen, 1998; Jones et al., 2004). In the following, z is the particle's height above the ground, and $f = 10^{-4}\ \mathrm{s^{-1}}$ is the Coriolis parameter, assumed constant with the typical value valid for mid-latitudes.

Stable conditions

$$\sigma_w = 1.3 u_* \left(1 - \frac{z}{h}\right) \tag{13}$$

$$t_{L_w} = 0.1 \frac{h}{\sigma_w} \left(\frac{z}{h}\right)^{0.8} \tag{14}$$

Neutral conditions

$$\sigma_w = 1.3 u_* \exp\left(-2\frac{fz}{u_*}\right) \tag{15}$$

$$t_{L_w} = \frac{0.5 z/\sigma_w}{1 + 15 f z/u_*} \tag{16}$$

Unstable conditions

If $\frac{z}{h} < 0.03$:

$$\frac{\sigma_w}{w_*} = 0.96 \left(3\frac{z}{h} - \frac{L}{h}\right)^{1/3} \tag{17}$$

If $0.03 \leq \frac{z}{h} < 0.4$:

$$\frac{\sigma_w}{w_*} = \min\left[0.96 \left(3\frac{z}{h} - \frac{L}{h}\right)^{1/3}, 0.763 \left(\frac{z}{h}\right)^{0.175}\right] \tag{18}$$

If $0.4 \leq \frac{z}{h} < 0.96$:

$$\frac{\sigma_w}{w_*} = 0.722 \left(1 - \frac{z}{h}\right)^{0.207} \tag{19}$$

If $0.96 \leq \frac{z}{h} < 1$:

$$\frac{\sigma_w}{w_*} = 0.37 \tag{20}$$

If $\frac{z}{h} < 0.1 \,\text{and}\, z > -L$:

$$t_{L_w} = \frac{0.1z}{\sigma_w[0.55 - 0.38z/L]} \tag{21}$$

If $\frac{z}{h} < 0.1 \,\text{and}\, z \leq -L$:

$$t_{L_w} = 0.59\frac{z}{\sigma_w} \tag{22}$$

If $\frac{z}{h} \geq 0.1$:

$$t_{L_w} = 0.15\frac{h}{\sigma_w}\left[1 - \exp\left(-5\frac{z}{h}\right)\right] \tag{23}$$

2.3 Plume rise algorithm

Two different plume rise algorithms have been implemented in the DERMA model; the Concawe formula and the Briggs formula. The former has the advantage that it is compatible with the current operational setup of DERMA, while the latter takes into account more meteorological considerations. A good overview and a comparison of the algorithms are given by Korsakissok and Mallet (2009). All quantities in the equations below are in SI units.

2.3.1 Concawe formula

The Concawe formula only takes the heat release as input and is, therefore, more general than the Briggs formulas described below. Further, its formulation makes it particularly interesting in the context of the DERMA model, because it can be directly implemented in the current operational setup. The plume rise Δh is calculated as (Brummage, 1968)

$$\Delta h = 0.071\frac{Q_h^{0.55}}{U^{0.67}}, \tag{24}$$

where Q_h is the heat release, and U is the model's horizontal wind speed at the height of the release, i.e. the stack height z_s. In the Kincaid experiment, however, the heat release needs to be calculated from the measurements of the exhaust velocity v_g, the gas temperature T_g, and the temperature of the ambient air T. The heat release is calculated as (Korsakissok and Mallet, 2009)

$$Q_h = 228.19 v_g d_s^2 (T_g - T), \tag{25}$$

where d_s is the stack diameter.

2.3.2 Briggs formulas

The Briggs formulas are specifically developed for gas being exhausted from a stack, and therefore both the exhaust velocity and the gas temperature are considered explicitly. Further, different formulations are used for different stability conditions. The formulas presented here are from (Briggs, 1965).

First, the static stability parameter s_p and the initial buoyancy flux parameter F_b are defined:

$$s_p = \frac{g}{T}\frac{\mathrm{d}\Theta}{\mathrm{d}z}\,, \quad F_b = g v_g d_s^2 \frac{T_g - T}{T_g}, \tag{26}$$

where g is the gravitational acceleration constant, and $\mathrm{d}\Theta/\mathrm{d}z$ is the gradient of the mean potential temperature. Since the algorithm is implemented in DERMA, the ambient air temperature T is here the model temperature instead of the observed as used for calculation of Q_h in Eq. (25).

In all cases, the plume rise is given by

$$\Delta h = \min(\Delta h_1, \Delta h_2), \tag{27}$$

where the stability dependent formulas for Δh_1 and Δh_2 are given below.

Stable conditions

$$\begin{aligned} \Delta h_1 &= 2.6\left(\frac{F_b}{U s_p}\right)^{1/3} \\ \Delta h_2 &= 4 F_b^{1/4} s_p^{-3/8} \end{aligned} \tag{28}$$

Unstable and neutral conditions

$$\begin{aligned} \Delta h_1 &= \begin{cases} 21.4\frac{F_b^{3/4}}{U} & \text{if } F_b < 55 \\ 38.71\frac{F_b^{3/5}}{U} & \text{if } F_b \geq 55 \end{cases} \\ \Delta h_2 &= \begin{cases} 4.3\left(\frac{F_b}{U w_*^2}\right)^{3/5} h^{2/5} & \text{unstable} \\ 1.54\left(\frac{F_b}{U u_*^2}\right)^{2/3} z_s^{1/3} & \text{neutral} \end{cases} \end{aligned} \tag{29}$$

2.3.3 Partial penetration of inversion layer

If the plume rise is large enough, or the PBL shallow enough, the plume may be lifted above the inversion layer at the top of the PBL. However, in some cases, the plume may only partially penetrate the inversion layer and leave a part of the plume trapped in the PBL. The formulas presented here are from Hanna and Paine (1989).

The penetration factor P, i.e. the fraction of the plume that penetrates the inversion layer is calculated as

$$P = 1.5 - \frac{\Delta z}{\Delta h}, \tag{30}$$

where Δh is the calculated plume rise and $\Delta z = h - z_s$. Note that the formulation of P allows for negative values as well as values larger than 1. However, as long as $P \leq 0$, the plume stays below the inversion layer, and when $P \geq 1$, the entire plume is above the inversion layer. Thus, only when $\Delta z/1.5 < \Delta h < 2\Delta z$, we need to account for partial penetration. When this is the case, the altered plume rise of the part trapped in the boundary layer is given by

$$\Delta h_{\text{below}} = (0.62 + 0.38P)\Delta z, \tag{31}$$

and the effective release rate is $Q_{\text{below}} = Q(1-P)$. However, Hanna and Paine (1989) do not provide a formula for calculating the height of the penetrating part of the plume. For this case, we assume

$$\Delta h_{\text{above}} = (1 + 0.38P)\Delta z, \tag{32}$$

and the effective release rate $Q_{\text{above}} = QP$, which gives a symmetric behavior around the boundary layer inversion. In practice, this is implemented by releasing the fraction $(1-P)$ of the puffs according to Eq. (31) and the fraction P of the puffs according to Eq. (32).

2.3.4 Initial puff size

Finally, the puffs' initial sizes will also be influenced by the plume rise. These are calculated as (Hanna and Paine, 1989)

$$\begin{aligned} \sigma_{y0} &= \frac{\Delta h}{3.5}, \\ \sigma_{z0} &= \frac{\Delta h}{2}. \end{aligned} \tag{33}$$

3 Model evaluation

The DERMA v2.0.0 model with the new elements described in Section 2 is evaluated against three different tracer gas experiments. For comparison, the model performance is compared to that of DERMA v1.0.0. For simplicity, we will refer to these as the "new" and "old" model versions throughout this section. First, the models are evaluated against the first European Tracer Experiment (ETEX), which has also previously been used for evaluation of DERMA (Graziani et al., 1998). Next, to evaluate the models' performances on shorter spatial scales, we use the Øresund experiment and the Kincaid experiment, which both consist of several releases on different days using varying measurement setups. In both experiments, the tracer concentrations are measured at ground level within the first 50 km downstream from the release location. The Kincaid experiment further provides a test case for the plume rise algorithms due to the large heat release associated with the release of the tracer. More details on the experiments and the data used are given in Section 3.1, 3.2, and 3.3. Next, Section 3.4 describes the experimental setup, and Section 3.5 presents and discusses the evaluation results.

3.1 The European tracer experiment

The European tracer experiment (ETEX) consisted of two releases, ETEX-1 and ETEX-2 (Graziani et al., 1998; Nodop et al., 1998). In the ETEX-1, which is used in this study, the non-decaying and non-depositing gas perfluoromethylcyclohexane

Figure 2. The three modelling domains used for the Harmonie simulations are indicated by the red squares in each plot. The upper plot shows the domain used for ETEX. The lower left plot shows the domain used for the Øresund experiment. The lower right plot shows the domain used for the Kincaid experiment. In all three plots, the red (and green in the case of the Øresund experiment) diamond shows the release location, and the black x's indicate the locations of sampling stations.

(PMCH) was used as a tracer, and a total of 340 kg of the gas was released to the atmosphere with a constant release rate during a 12-hour period starting at 16.00 UTC on 23 October 1994.

The gas was released near Monterfil in Brittany, France, from 8 meters above the ground, see Figure 2. The gas was then sampled over 30 three-hour intervals by a network of 168 ground-level sampling stations distributed in 17 European countries. The ETEX observation data set is available via https://remon.jrc.ec.europa.eu/past_activities/etex/site/index.html (latest access March 12, 2024).

3.2 The Øresund experiment

The Øresund experiment consisted of nine non-buoyant sulfur hexafluoride (SF6) releases on different days from 16 May to 14 June 1984 (Mortensen and Gryning, 1989). Six releases were made from Barsebäck in Sweden (from 95 m above the ground), and three from the Gladsaxe mast in Denmark (from 115 m above the ground), release locations are shown in Figure 2. In each of the releases, the release location was chosen based on the wind direction, such that the tracer was released near the upwind coast of Øresund and was sampled by a network of ground-based stations on the opposite coast. The sampling stations were typically configured in an arc near the coast and one or more arcs further inland. The dataset is thoroughly described by Mortensen and Gryning (1989) and is publicly available from https://doi.org/10.5281/zenodo.161966 (latest access March 12, 2024).

In this study, we use all the available ground-based measurements, but when possible, measurements adjacent in time are averaged to provide average concentrations over longer time periods. This was done to reduce noise from the relatively short sampling periods (down to 15 minutes). For illustration, Figure 3 shows the model predictions together with observations for a selected time during one of the Øresund releases. The example is not randomly selected but rather serves as a case demonstrating how the model improvements, in some scenarios, give a more realistic dispersion pattern.

3.3 The Kincaid experiment

The Kincaid experiment consists of a series of SF6 releases spread out over three roughly one-month-long periods in 1980 and 1981 (Bowne and Londergan, 1983). The gas was released from the 187 m high stack of the Kincaid power plant, located in Illinois, USA, see Figure 2. In the surrounding area, primarily consisting of flat farmland with some lakes, air concentrations were sampled over one-hour periods by a network consisting of roughly 1500 potential sampling locations distributed in 12 arcs in varying distances from 0.5 km up to 50 km downwind of the source. Not all samplers were active at all times, so the number of measurement locations varies. The SF6 tracer was released through the stack of the power plant, and the high gas temperatures often resulted in a substantial effective plume rise. The gas temperature and the exhaust velocity were measured and are available as well as relevant meteorological observations from a nearby weather mast (Bowne and Londergan, 1983).

The Kincaid data exist in different versions. One data set is distributed as part of the Model Validation Kit (MVK) described by Olesen (2005), which is available via https://www.harmo.org/kit.php (latest access March 12, 2024). Another version of the Kincaid data set was structured by John Irving and was distributed via his website, now maintained by the Harmo organization, https://www.harmo.org/jsirwin (latest access March 12, 2024).

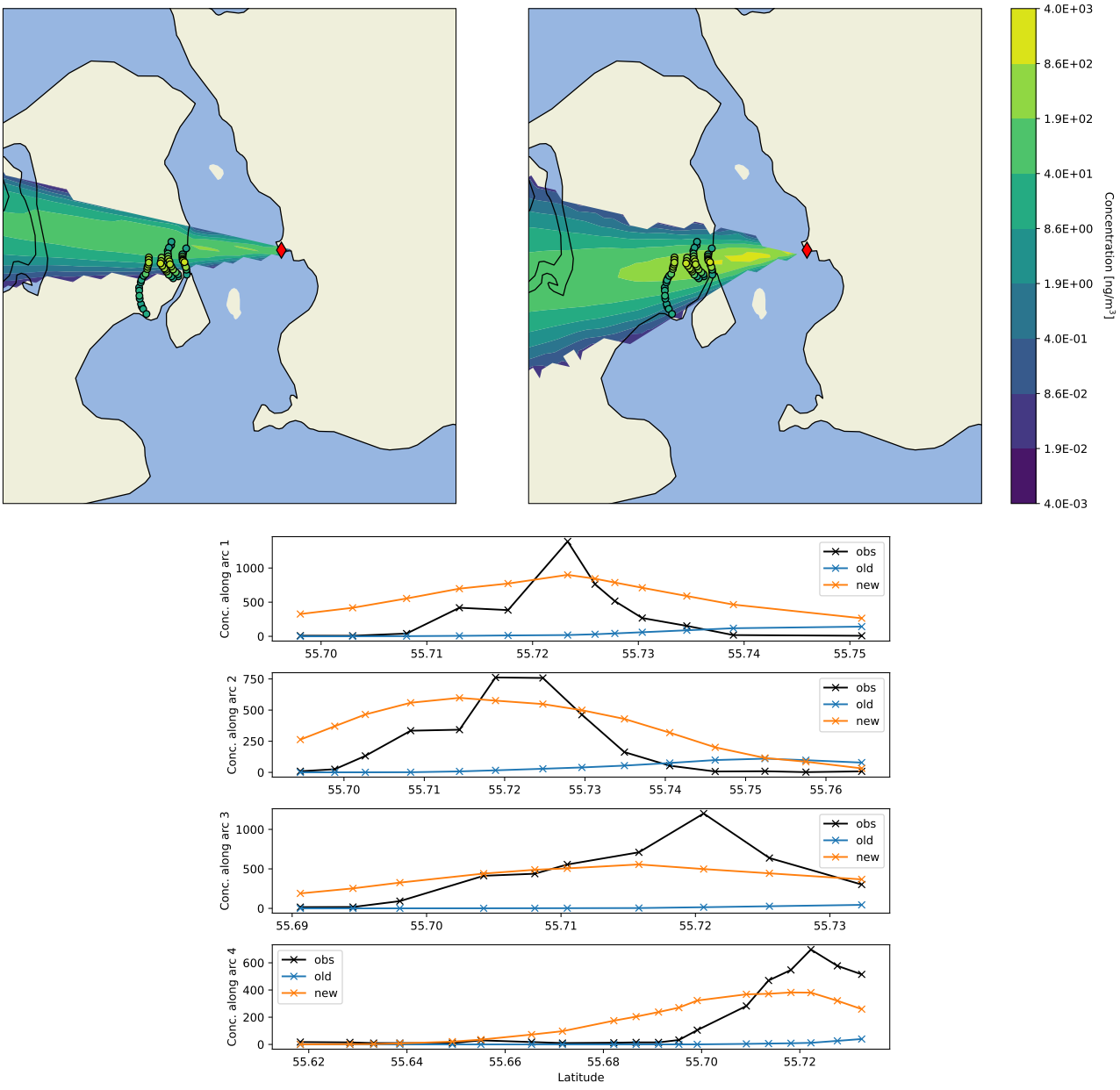

Figure 3. Examples of results are shown for a selected dispersion scenario for the Øresund experiment. The measurements and model results show average air concentrations during the interval 10 UTC to 11 UTC, 6 June 1984. In the upper plots, the plumes show the model results of both the old (left) and new (right) models, while the dots show the measured values. In the lower plot, observations are shown together with model predictions at the measurement locations. The arcs are numbered from 1 to 4, with 1 being the arc closest to the release location.

As discussed by Olesen (2005), the concentration patterns were often irregular, with high and low values simultaneously occurring along the same arc. To provide a more robust foundation for model evaluation, arcwise maxima have been estimated along with a quality indicator ranging from 0 to 3 indicating how reliable each arcwise maximum is. The two above mentioned versions of the data set differ slightly due to different algorithms used for assigning sampling stations to arcs as well as to assessing the quality of measurements, see discussion https://www.harmo.org/jsirwin/KincaidHourlyDiscussion.html (latest access March 12, 2024). In this study, we use the version from John Irving, and both the entire set of SF6 measurements and the quality-controlled arcwise maximum values are used for the validation.

3.4 Experimental setup

For all three experiments, the simulations have been carried out using meteorological data from the limited-area NWP model Harmonie (Bengtsson et al., 2017). We use a horizontal grid resolution of approximately 2 km and a terrain-influenced hybrid vertical coordinate with 65 levels. The domains used for the simulations are shown in Figure 2. For initial conditions and spatial boundary conditions, we use the ERA5 reanalysis (Hersbach et al., 2020).

Both the versions of DERMA have then been run for all three experiments. For the Kincaid experiment, the new model version was run with both of the plume rise algorithms described in Section 2.3. In all experiments, we use advection time steps of three minutes, and the sources have been discretized by releasing 50 puffs at every time step during the release period.

The resulting concentration fields have been interpolated in space using bilinear interpolation, and integrated in time to obtain a list of modelled average concentrations corresponding to the set of observations. Denoting the observations $\mathbf{x}$ and the predictions $\mathbf{y}$, we define the following statistical parameters used for model validation (cf. Draxler et al., 2001)

$$
\begin{aligned}
\mathrm{rmse} &= \sqrt{\frac{1}{N}\sum_i (y_i - x_i)^2}, \\
\mathrm{nmse} &= \frac{1}{N\mu_{\mathbf{x}}\mu_{\mathbf{y}}}\sum_i (y_i - x_i)^2, \\
\mathrm{r} &= \frac{(\mathbf{x}-\mu_{\mathbf{x}})\cdot(\mathbf{y}-\mu_{\mathbf{y}})}{\sigma_{\mathbf{x}}\sigma_{\mathbf{y}}}, \\
\mathrm{b} &= \frac{1}{N}\sum_i y_i - x_i, \\
\mathrm{fb} &= \frac{2b}{\mu_{\mathbf{x}}+\mu_{\mathbf{y}}}, \\
\mathrm{fms} &= 100\frac{N(y>0)\cap N(x>0)}{N(y>0)\cup N(x>0)}, \\
\mathrm{foex} &= 100\left(\frac{N_{(y_i>x_i)}}{N} - \frac{1}{2}\right), \\
\mathrm{fa}_2 &= 100\left(\frac{N_{(1/2<y_i/x_i<2)}}{N}\right), \\
\mathrm{fa}_5 &= 100\left(\frac{N_{(1/5<y_i/x_i<5)}}{N}\right),
\end{aligned}
\tag{34}
$$

where μ and σ are the mean and standard deviation, rmse is the root mean square error, nmse is the normalized mean square error, r is the Pearson correlation coefficient, and b mean bias. Further, fb is the fractional bias, which is a normalized measure of the mean bias ranging from -2 to 2, fms is the figure of merit in space, which is defined as the percentage of overlap between the measured and predicted areas, foex is a measure of how many predictions are over-/underestimated, it is centered around zero and ranges from -50% to 50%. Finally, fa_α is the percentage of the predictions that are within a factor of $1/\alpha$ to α from the observation. For the calculation of foex and fa_α, the 0-0 pairs are excluded. Due to the infinite nature of Gaussian distributions, a puff model technically always has non-zero predictions everywhere. For that reason, model predictions lower than the detection limit for each experiment are interpreted as non-detections.

3.5 Evaluation results

For all three experiments, the statistical parameters Eq. (34) have been calculated and are shown in the tables 1-3. In Figures 4-6, scatter plots of the model predictions as a function of the observed values are shown, as well as quantile-quantile plots of predictions vs observations. For the Kincaid experiment, the model is further evaluated using the arcwise maximum values with quality indicator 3 (best quality), shown in Table 4 and Figure 7.

Table 1. Statistical parameters Eq. (34) calculated for ETEX.

	mean	std	rmse	nmse	r	b	fb	fms	foex	fa_2	fa_5
Observations	0.10	0.44	0.00	0.00	1.00	0.000	0.00	100.0	0.0	100.0	100.0
DERMA v1.0.0	0.13	0.63	0.57	24.42	0.47	0.023	0.19	55.8	-4.0	20.8	40.5
DERMA v2.0.0	0.10	0.60	0.53	26.78	0.52	-0.005	-0.05	55.8	-14.5	23.8	43.6

From Table 1, we see that the performances of the old and new models are quite similar for the ETEX experiment. The new model does show a slight improvement for the parameters r, b and fb, fa_2 and fa_5. For the other parameters, the old model performs slightly better, but the differences are very small in general, which is expected because the long-range formulation of the new hybrid approach is similar to that of the old DERMA model, and there are few measurement stations close to the release point. From the scatter plots in Figure 4, it does look like the new model has slightly less spread for higher values, while the quantile-quantile plots are very similar. Some statistical parameters, such as fa_2 and fa_5, may suggest a low level of agreement between the model predictions and observations. However, it is important to recognize that the Gaussian nature of the concentration distribution implies that even small shifts in plume position can produce large local discrepancies in surface concentration. Further, these statistical parameters are consistent with those reported in the original model evaluation and, thus, fall within the expected range (Graziani et al., 1998).

The improved performance for long-range dispersion can likely be explained by the new stochastic transport scheme described in Section 2.1.2.

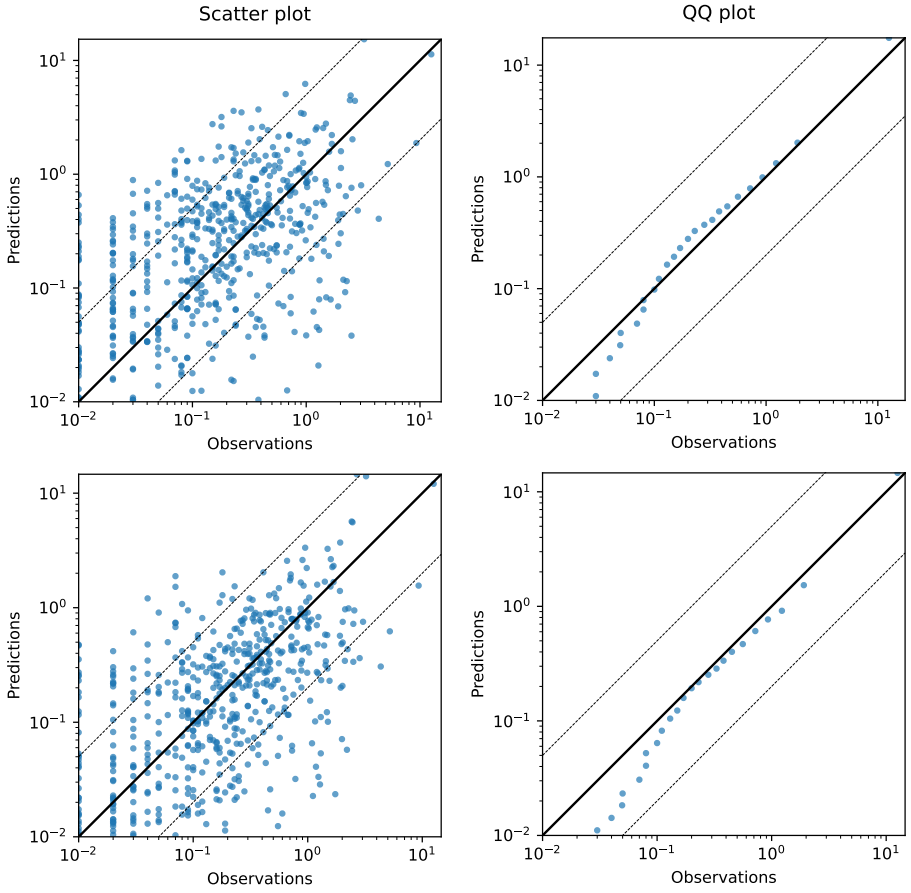

Figure 4. Results for the evaluation against ETEX. (left) scatter plot of model predictions as a function of observations, and (right) Quantile-quantile plot. Concentrations are in $[\mathrm{ng\,m^{-3}}]$. The upper figures are for the old version of DERMA, and the lower figures are for the new version. The solid black line indicates a perfect linear fit and the dashed lines indicate deviations of a factor 5 and 1/5 away from the observation.

Table 2. Statistical parameters Eq. (34) calculated for the Øresund experiment. When possible, longer time averages have been calculated to reduce the noise arising from the very short sampling periods, see Section 3.2 for further details.

	mean	std	rmse	nmse	r	b	fb	fms	foex	fa_2	fa_5
Observations	114.30	213.80	0.00	0.00	1.00	0.00	0.00	100.0	0.0	100.0	100.0
DERMA v1.0.0	29.31	48.53	231.09	15.94	0.09	-84.99	-1.18	51.5	-31.2	14.5	32.5
DERMA v2.0.0	131.46	186.30	229.13	3.49	0.35	17.16	0.14	74.1	-6.4	24.9	47.7

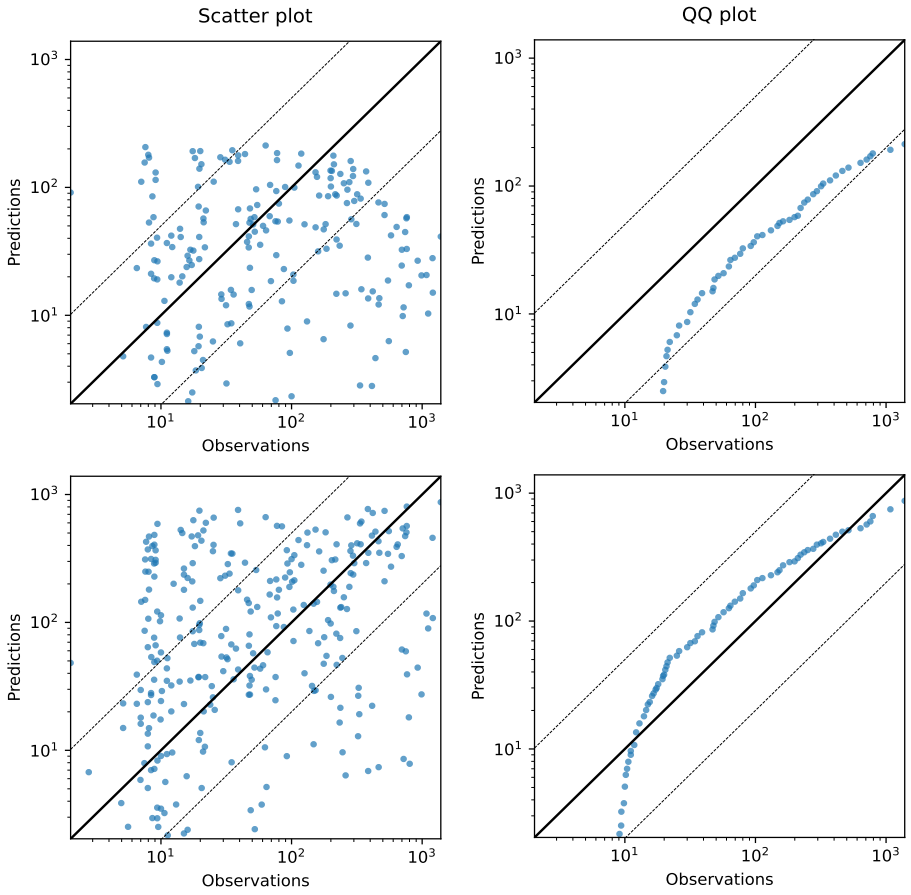

Figure 5. Results for the evaluation against the Øresund experiment. (left) scatter plot of model predictions as a function of observations, and (right) Quantile-quantile plot. Concentrations are in $[\mathrm{ng\,m^{-3}}]$. The upper figures are for the old version of DERMA, and the lower figures are for the new version. The solid black line indicates a perfect linear fit and the dashed lines indicate deviations of a factor 5 and 1/5 away from the observation.

From Table 2, we see that the ground concentrations predicted by the old DERMA model are systematically underestimated for the Øresund experiment. This is in accordance with the expectations due to the instantaneous vertical mixing throughout the PBL, which will cause lower concentrations near the source. In reality, the gas was released quite close to the ground, and we would therefore expect the ground concentrations to be high near the source. Essentially, the new model performs better across all statistical parameters, and the same is indicated by Figure 5. Although none of the models correlate particularly well with the observations, the new model does predict high observed concentrations better, whereas the old model underestimates all the higher concentrations. The quantile-quantile plot also indicates that the new model is better on average, although it overestimates lower values and underestimates the highest observations.

For the Kincaid experiment, we first consider the results based on the full measurement data set. Table 3 shows that the old model systematically overestimates the ground concentrations with a mean concentration of approximately 360 $\mathrm{ng\,m^{-3}}$, whereas the mean of the observations is roughly 54 $\mathrm{ng\,m^{-3}}$. This is again in accordance with the expectations; due to the plume rise, the effective release height is often quite high above the surface, and therefore the ground concentrations should be low near the source, whereas the old model mixes the tracer down to the surface from the start. The new version also has a positive bias, but the magnitude depends strongly on the plume rise algorithm used. The results obtained by using Briggs' formula give only a very small bias (average concentration of 60 $\mathrm{ng\,m^{-3}}$), while the results obtained by using the Concawe formula have an average of 112 $\mathrm{ng\,m^{-3}}$. The remaining statistics are quite similar for the two new models, and for rmse, nmse, r, b and fb the performance is significantly better than for the old model, while for the remaining statistics, there seems to be only a small improvement. Figure 6 also shows that there is a very large spread in the scatter plots for all three models. However, the quantile-quantile plots do suggest a significantly better representation of the concentration field with the new model, especially when using the Briggs plume rise scheme.

Table 3. Statistical parameters Eq. (34) calculated for the Kincaid experiment using all available measurements.

	mean	std	rmse	nmse	r	b	fb	fms	foex	$\mathrm{fa_2}$	$\mathrm{fa_5}$
Observations	53.87	171.12	0.00	0.00	1.00	0.00	0.00	100.0	0.0	100.0	100.0
DERMA v1.0.0	360.44	1160.86	1205.80	74.89	0.04	306.58	1.48	29.2	29.9	8.1	16.9
DERMA v2.0.0 (Briggs)	60.29	216.25	246.82	18.76	0.20	6.43	0.11	31.9	11.7	8.7	18.4
DERMA v2.0.0 (Concawe)	112.05	326.12	332.81	18.35	0.25	58.19	0.70	32.9	21.0	9.4	19.5

Table 4. Statistical parameters Eq. (34) calculated for the Kincaid experiment using the arcwise maximum values with quality flag 3.

	mean	std	rmse	nmse	r	b	fb	foex	$\mathrm{fa_2}$	$\mathrm{fa_5}$
Observations	41.03	35.03	0.00	0.00	1.00	0.00	0.000	0.0	100.0	100.0
DERMA v1.0.0	66.30	84.99	89.06	2.92	0.19	25.27	0.471	13.5	53.3	85.1
DERMA v2.0.0 (Briggs)	27.37	35.41	47.16	1.98	0.18	-13.66	-0.399	-19.1	32.3	63.2
DERMA v2.0.0 (Concawe)	46.48	50.37	49.74	1.30	0.37	5.45	0.124	-1.3	43.6	76.6

It should be noted that this comparison method is very sensitive to even small errors in the meteorological model data; since the spatial and temporal resolution of the measurements is so high, an error in e.g. the wind direction may result in large errors. Therefore, a more robust way of evaluating the model may be to compare model predictions with the arcwise maximum values. As described in Section 3.3, there were up to 12 arcs at distances 0.5 km, 1 km, 2 km, 3 km, 5 km, 7 km, 10 km, 15 km, 20 km, 30 km, 40 km and 50 km (not all arcs exist for all release periods). For every one-hour sampling period, the maximum

value in each available arc is provided along with a quality indicator from 0 to 3. For the comparison, the predicted maximum concentration of each arc was estimated by first interpolating the concentration field to all sampling locations of that arc, and then calculating the maximum value. The results in Table 4 and Figure 7 are based only on maximum values with quality indicator 3.

From Table 4, the results are slightly more ambiguous than from the previous comparisons. The new model using Briggs' formula performs slightly better than the old model for the parameters nmse, b and fb, while the old model performs slightly better for foex, fa_2 and fa_5. However, the new model using the Concawe formula seems to stand out with better performance on all parameters except for fa_2 and fa_5, where the old model performs slightly better. Generally, all models perform much better on the arcwise maxima than when using the entire dataset, which confirms that this approach is less sensitive to, e.g., errors in the predicted wind direction. From Figure 7, we also see that all three scatter plots have a much smaller spread than in Figure 6.

Finally, it is relevant to note that there is quite a large difference in performance between the two new versions, which are identical except for the plume rise scheme used. This clearly indicates the importance of estimating the start height correctly in order to predict reliable ground concentrations near the source.

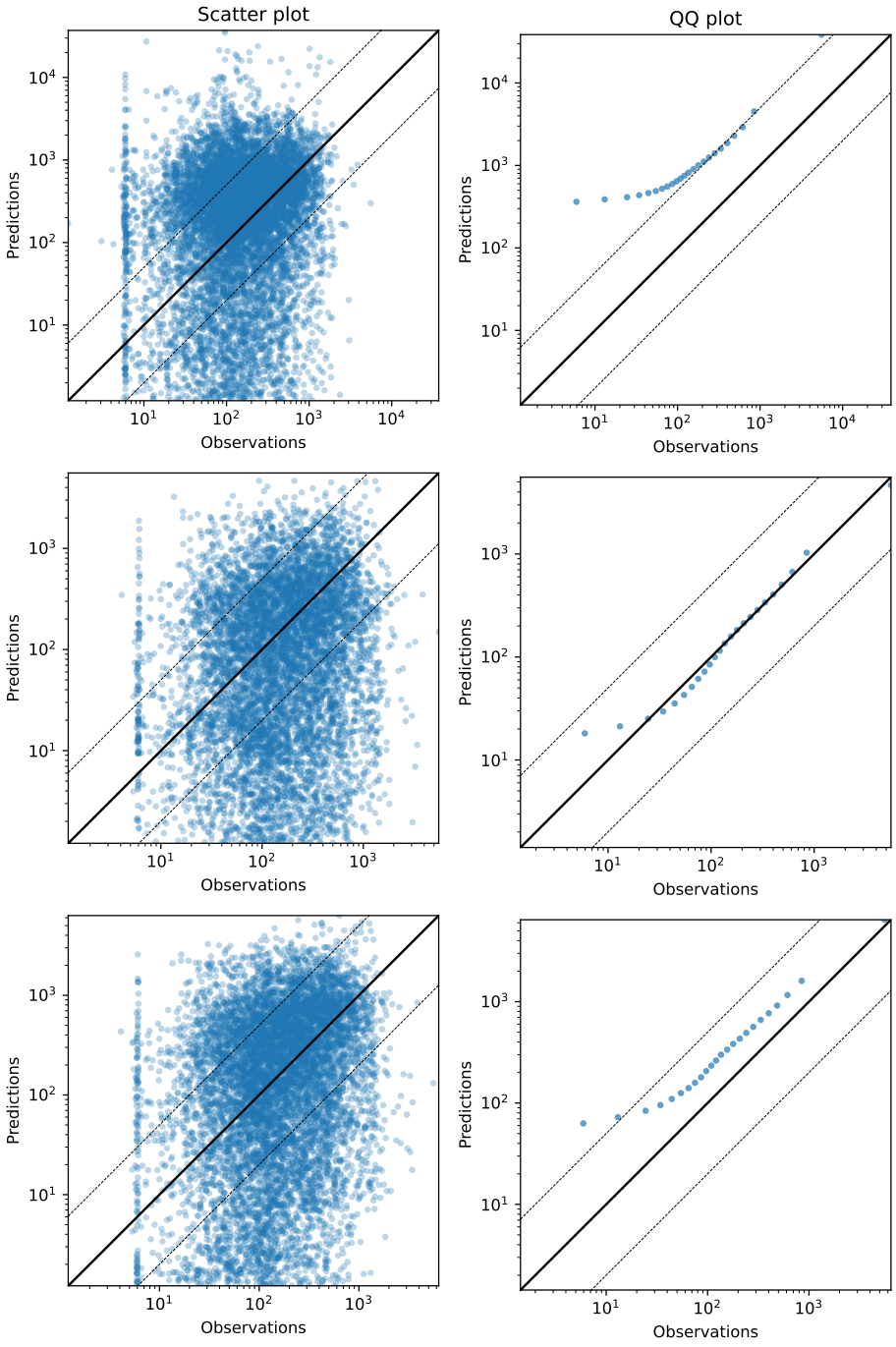

Figure 6. Results for the evaluation against the Kincaid experiment using all available measurements. (left) scatter plot of model predictions as a function of observations, and (right) Quantile-quantile plot. Concentrations are in $[\mathrm{ng\,m^{-3}}]$. The upper figures are for the old version of DERMA, the middle figures are for the new version using the Briggs plume rise formula, and the lower figures are for the new version using the Concawe formula. The solid black line indicates a perfect linear fit and the dashed lines indicate deviations of a factor 5 and 1/5 away from the observation.

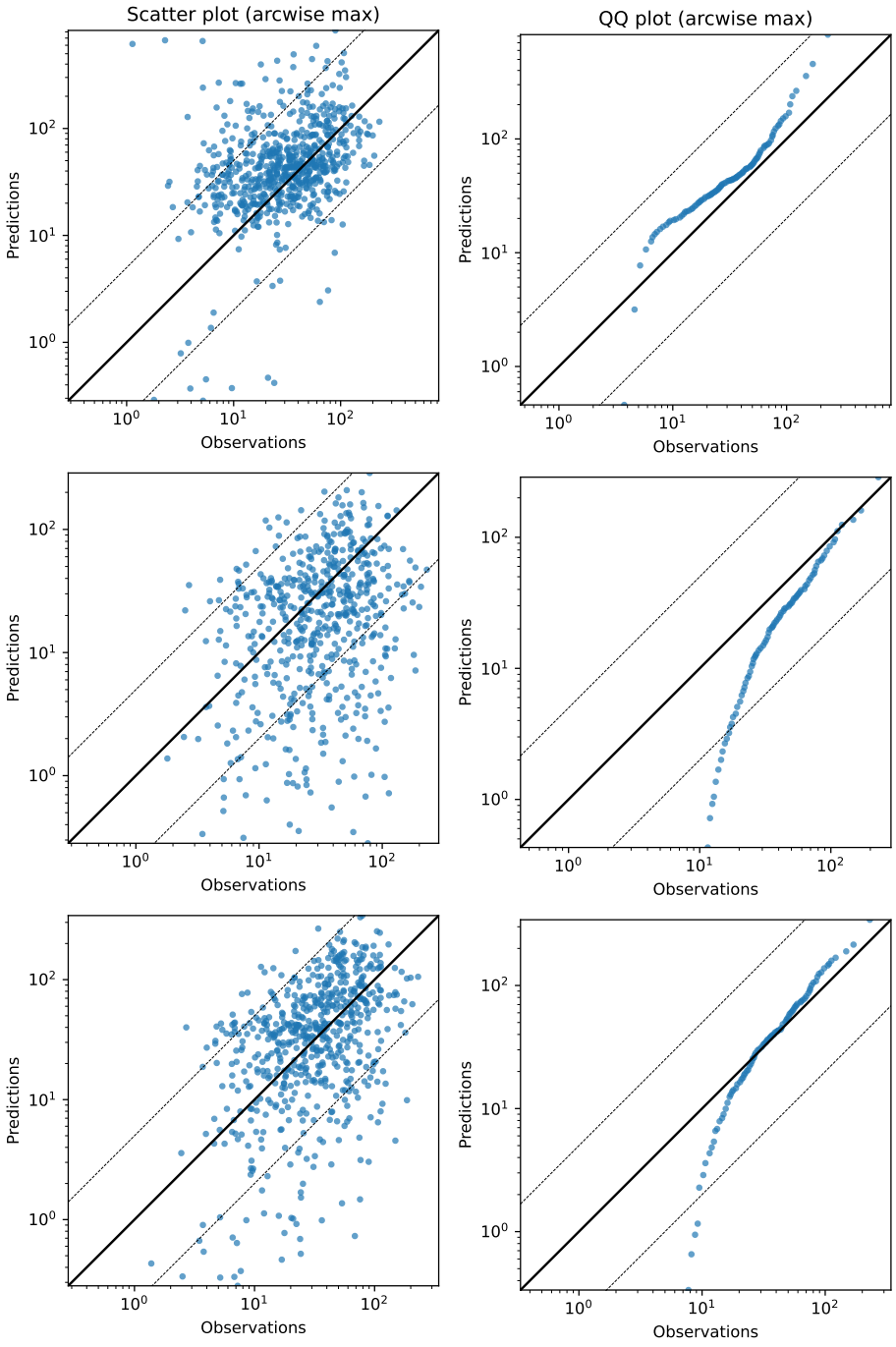

Figure 7. Results for the evaluation against the Kincaid experiment using arcwise maximum values with quality flag 3. (left) scatter plot of model predictions as a function of observations, and (right) Quantile-quantile plot. Further, concentrations have been divided by the mean release rate for the given release. The upper figures are for the old version of DERMA, the middle figures are for the new version using the Briggs plume rise formula, and the lower figures are for the new version using the Concawe formula. The solid black line indicates a perfect linear fit and the dashed lines indicate deviations of a factor 5 and 1/5 away from the observation.

4 Summary and conclusions

This paper describes a new hybrid particle-puff formulation for dispersion modelling, making use of simple assumptions to separate turbulence into a stochastic particle part and a puff part, without the theoretical risk of double counting turbulent effects. This formulation allows for the use of a limited number of puffs and longer advection time steps compared to stochastic particle models. Further, compared to the classical puff approach, it allows for a more realistic description of turbulent diffusion for small puffs. For large puffs, on the other hand, the formulation allows puffs to be exposed to the vertical wind shear in the PBL without the need for puff splitting.

In addition, new parameterizations have been implemented in DERMA for turbulent wind fluctuation and Lagrangian time scales, for PBL height, and for plume rise. For the latter, both the Concawe formula and the Briggs formula have been implemented.

The model evaluation shows that implementation of the new hybrid approach improves the performance of DERMA for all three considered experiments. The evaluation method is not very robust, since the model predictions are very sensitive to meteorological errors. However, since our evaluation uses a large amount of measurement data sampled over many days during different times of the year, the overall trends in the results should give a good indication of the models' performances. Further, the use of the arcwise maxima from the Kincaid experiment provides a completely different way of comparing model predictions with observations, which again indicates improved performance when using the new hybrid formulation.

Further, a comparison of the two plume rise algorithms indicates how important it is to correctly estimate the initial plume height in order to predict the ground concentrations near the source. Unfortunately, there is no clear answer to which plume rise algorithm is best; in our evaluation, the Briggs formulas seem to give slightly better results when calculating statistics based on all data, while the Concawe formula performs better when compared to the arcwise maxima. However, the Concawe formula is somewhat more generally applicable, because it only needs the released heat, whereas the Briggs formulas are specifically developed for gas being exhausted from a stack and both gas temperature and exhaust velocity are necessary inputs.

In conclusion, the developed hybrid particle-puff formulation, in combination with the additional new implementations, has improved the performance of DERMA, especially for short-range dispersion modelling. Hence, these improvements could pave the way for new applications of the DERMA model in the future.

Code and data availability. All measurement data used are already publicly available. The KINCAID data are available via https://www.harmo.org/jsirwin/Tracer_Data.html (latest access March 12, 2024). The Øresund experiment data are available via https://doi.org/10.5281/zenodo.161966 (latest access March 12, 2024). The ETEX observation data are available via https://remon.jrc.ec.europa.eu/past_activities/etex/site/index.html (latest access March 12, 2024). The ERA5 data are available via the https://www.ecmwf.int/en/forecasts/datasets/reanalysis-datasets/era5 (latest access March 12, 2024). The meteorological data produced by Harmonie is archived in DMI's storage facility but cannot easily be made publicly available due to the large data amount (more than 2 TB data). It can be shared upon reasonable request, if a suitable practical solution can be found. Unfortunately, the code cannot be published, because the DERMA model is not publicly available.

Author contributions. KST developed the methodology, implemented it into the DERMA model, and carried out the model evaluation. Conceptualization and design of the DERMA experiments were carried out by KST and JHS. KST prepared the manuscript with contributions from JHS.

Competing interests. The authors declare that they have no conflict of interest.

Acknowledgements. This work was developed as part of the PhD thesis of the corresponding author, KST. The PhD was carried out in collaboration between the Danish Meteorological Institute and the Niels Bohr Institute, University of Copenhagen. We would like to acknowledge the support from both institutions as well as the Innovation Fund Denmark for funding the project through grant nr 196-00017B.

References

Andronopoulos, S., Davakis, E., and Bartzis, J. G.: RODOS-DIPCOT model description and evaluation, Report RODOS (RA2)-TN (09), 1, 2009.

Baklanov, A. and Sørensen, J. H.: Parameterisation of radionuclide deposition in atmospheric dispersion models, Phys. Chem. Earth, 26, 787–799, https://doi.org/10.1016/S1464-1909(01)00087-9, 2001.

Bengtsson, L., Andrae, U., Aspelien, T., Batrak, Y., Calvo, J., de Rooy, W., Gleeson, E., Hansen-Sass, B., Homleid, M., Hortal, M., Ivarsson, K.-I., Lenderink, G., Niemelä, S., Nielsen, K. P., Onvlee, J., Rontu, L., Samuelsson, P., Muñoz, D. S., Subias, A., Tijm, S., Toll, V., Yang, X., and Ødegaard Køltzow, M.: The HARMONIE–AROME Model Configuration in the ALADIN–HIRLAM NWP System, Monthly Weather Review, 145, 1919–1935, https://doi.org/10.1175/MWR-D-16-0417.1, 2017.

Bowne, N. and Londergan, R.: Overview, results, and conclusions for the EPRI Plume-Model Validation and Development Project: plains site. Final report, Tech. rep., TRC Environmental Consultants, Inc., East Hartford, CT (USA), https://www.osti.gov/biblio/6092793, 1983.

Briggs, G. A.: A plume rise model compared with observations, Journal of the Air Pollution Control Association, 15, 433–438, https://doi.org/10.1080/00022470.1965.10468404, 1965.

Bromiley, P.: Products and convolutions of Gaussian probability density functions, Tina-Vision Memo, 3, 1, 2003.

Brummage, K.: The calculation of atmospheric dispersion from a stack, Atmospheric Environment (1967), 2, 197–224, https://doi.org/10.1016/0004-6981(68)90049-8, 1968.

De Haan, P. and Rotach, M. W.: A novel approach to atmospheric dispersion modelling: The Puff-Particle Model, Quarterly Journal of the Royal Meteorological Society, 124, 2771–2792, https://doi.org/10.1007/978-1-4615-5841-5_45, 1998.

Draxler, R. R. and Hess, G.: Description of the HYSPLIT4 modeling system, 1997.

Draxler, R. R., Heffter, J. L., and Rolph, G. D.: Data archive of tracer experiments and meteorology, Tech. rep., Citeseer, https://www.arl.noaa.gov/hysplit/datem-tracer-evaluation/datem/, 2001.

Gifford, F.: The random force theory: Application to meso-and large-scale atmospheric diffusion, Boundary-Layer Meteorology, 30, 159–175, https://doi.org/10.1007/BF00121953, 1984.

Gloster, J., Jones, A., Redington, A., Burgin, L., Sørensen, J. H., Turner, R., Hullinger, P., Dillon, M., Astrup, P., Garner, G., D'Amours, R., Sellers, R., and Paton, D.: Airborne spread of foot-and-mouth disease – model intercomparison, Veterinary Journal, 183, 278–286, https://doi.org/10.1016/j.tvjl.2008.11.011, 2010.

Graziani, G., Klug, W., and Mosca, S.: Real-time long-range dispersion model evaluation of the ETEX first release, Office for Official Publications of the European communities, https://op.europa.eu/en/publication-detail/-/publication/ae88ef74-f74b-495e-aea4-5a278ba08700, 1998.

Hanna, S.: Applications in air pollution modeling, in: Atmospheric Turbulence and Air Pollution Modelling: A Course held in The Hague, 21–25 September, 1981, pp. 275–310, Springer, https://doi.org/10.1007/978-94-010-9112-1_7, 1984.

Hanna, S. R. and Paine, R. J.: Hybrid plume dispersion model (HPDM) development and evaluation, Journal of Applied Meteorology and Climatology, 28, 206–224, https://doi.org/10.1175/1520-0450(1989)028<0206:HPDMDA>2.0.CO;2, 1989.

Hersbach, H., Bell, B., Berrisford, P., Hirahara, S., Horányi, A., Muñoz-Sabater, J., Nicolas, J., Peubey, C., Radu, R., Schepers, D., et al.: The ERA5 global reanalysis, Quarterly Journal of the Royal Meteorological Society, 146, 1999–2049, https://doi.org/10.1002/qj.3803, 2020.

Hoe, S., Müller, H., Gering, F., Thykier-Nielsen, S., and Sørensen, J. H.: ARGOS 2001 a decision support system for nuclear emergencies, In: Proceedings of the Radiation Protection and Shielding Division Topical Meeting. April 14–17. Santa Fe, New Mexico, USA, https://orbit.dtu.dk/en/publications/argos-decision-support-system-for-emergency-management, 2002.

Jones, A., Thomson, D., Hort, M., and Devenish, B.: The UK Met Office's next-generation atmospheric dispersion model, NAME III, in: Air Pollution Modeling and its Application XVII, Proceedings of the 27th NATO/CCMS International Technical Meeting on Air Pollution Modelling and its Application, pp. 24–29, https://doi.org/10.1007/978-0-387-68854-1_62, 2004.

Kolmogorov, A. N.: The local structure of turbulence in incompressible viscous fluid for very large Reynolds, Numbers. In Dokl. Akad. Nauk SSSR, 30, 301, https://doi.org/10.1098/rspa.1991.0075, 1941.

Korsakissok, I. and Mallet, V.: Comparative study of Gaussian dispersion formulas within the Polyphemus platform: evaluation with Prairie Grass and Kincaid experiments, Journal of applied meteorology and climatology, 48, 2459–2473, https://doi.org/10.1175/2009JAMC2160.1, 2009.

Mikkelsen, T., Alexandersen, S., Astrup, P., Champion, H. J., Donaldson, A. I., Dunkerley, F. N., Gloster, J., Sørensen, J. H., and Thykier-Nielsen, S.: Investigation of airborne foot-and-mouth disease virus transmission during low-wind conditions in the early phase of the UK 2001 epidemic, Atmos. Chem. Phys, 3, 2101–2110, https://doi.org/10.5194/acp-3-2101-2003, 2003.

Mortensen, N. G. and Gryning, S.-E.: The Øresund Experiment Data Bank Report, Department of Meteorology and Wind Energy, Risø National Laboratory, https://orbit.dtu.dk/en/publications/the-%C3%B8resund-experiment-data-bank-report, 1989.

Nodop, K., Connolly, R., and Girardi, F.: The field campaigns of the European Tracer Experiment (ETEX): Overview and results, Atmospheric Environment, 32, 4095–4108, https://doi.org/10.1016/S1352-2310(98)00190-3, 1998.

Olesen, H.: User´s guide to the Model Validation Kit, Research Notes from NERI, National Environmental Research Institute, https://pure.au.dk/portal/en/publications/users-guide-to-the-model-validation-kit, 2005.

Pisso, I., Sollum, E., Grythe, H., Kristiansen, N. I., Cassiani, M., Eckhardt, S., Arnold, D., Morton, D., Thompson, R. L., Groot Zwaaftink, C. D., et al.: The Lagrangian particle dispersion model FLEXPART version 10.4, Geoscientific Model Development, 12, 4955–4997, https://doi.org/10.5194/gmd-12-4955-2019, 2019.

Scire, J. S., Strimaitis, D. G., Yamartino, R. J., et al.: A user's guide for the CALPUFF dispersion model, Earth Tech, Inc, 521, 1–521, 2000.

Sørensen, J. H.: Sensitivity of the DERMA long-range Gaussian dispersion model to meteorological input and diffusion parameters, Atmospheric Environment, 32, 4195–4206, https://doi.org/10.1016/S1352-2310(98)00178-2, 1998.

Sørensen, J. H.: Method for source localization proposed and applied to the October 2017 case of atmospheric dispersion of Ru-106, Journal of environmental radioactivity, 189, 221–226, https://doi.org/10.1016/j.jenvrad.2018.03.010, 2018.

Sørensen, J. H., Mackay, D. K. J., Jensen, C. Ø., and Donaldson, A. I.: An integrated model to predict the atmospheric spread of foot-and-mouth disease virus, Epidemiol. Infect., 124, 577–590, https://doi.org/10.1017/S095026889900401X, 2000.

Sørensen, J. H., Jensen, C. Ø., Mikkelsen, T., Mackay, D., and Donaldson, A. I.: Modelling the atmospheric spread of foot-and-mouth disease virus for emergency preparedness, Phys. Chem. Earth, 26, 93–97, https://doi.org/10.1016/S1464-1909(00)00223-9, 2001.

Sørensen, J. H., Baklanov, A., and Hoe, S.: The Danish emergency response model of the atmosphere (DERMA), Journal of environmental radioactivity, 96, 122–129, https://doi.org/10.1016/j.jenvrad.2007.01.030, 2007.

Stohl, A., Forster, C., Frank, A., Seibert, P., and Wotawa, G.: The Lagrangian particle dispersion model FLEXPART version 6.2, Atmospheric Chemistry and Physics, 5, 2461–2474, https://doi.org/10.5194/acp-5-2461-2005, 2005.

Thykier-Nielsen, S., Deme, S., and Mikkelsen, T.: Description of the atmospheric dispersion module RIMPUFF, Riso National Laboratory, PO Box, 49, 1999.

Tølløse, K. S. and Sørensen, J. H.: Bayesian Inverse Modelling for Probabilistic Multi-Nuclide Source Term Estimation Using Observations of Air Concentration and Gamma Dose Rate, Atmosphere, 13, 1877, https://doi.org/10.3390/atmos13111877, 2022.

Tølløse, K. S., Kaas, E., and Sørensen, J. H.: Probabilistic Inverse Method for Source Localization Applied to ETEX and the 2017 Case of Ru-106 including Analyses of Sensitivity to Measurement Data, Atmosphere, 12, https://doi.org/10.3390/atmos12121567, 2021.

Vogelezang, D. and Holtslag, A.: Evaluation and model impacts of alternative boundary-layer height formulations, Boundary-Layer Meteorology, 81, 245–269, https://doi.org/10.1007/BF02430331, 1996.

Zannetti, P.: Air pollution modeling: theories, computational methods and available software, Springer Science & Business Media, 2013.